Relative Corrosion Reactivity and Surface Microstructure of $YBa_2Cu_3O_{7-x}$ Samples with Different Oxygen Contents

Ji-Ping Zhou, David R. Riley, and John T. McDevitt*

Department of Chemistry and Biochemistry, The University of Texas at Austin, Austin, Texas 78712-1167

Received June 10, 1992. Revised Manuscript Received December 22, 1992

The relative chemical reactivity toward water within the $YBa_2Cu_3O_{7-x}$ series ($0 < x < 1$) is found to be $YBa_2Cu_3O_{6.59} < YBa_2Cu_3O_{7.00} \ll YBa_2Cu_3O_{6.05}$. Thus, factors other than copper valence, such as internal strain and lattice vacancies, are likely to be responsible for the high reactivity of the oxygen-deficient phase. For the two orthorhombic samples, $YBA_2Cu_3O_{7.00}$ and $YBa_2Cu_3O_{6.59}$, the reactivity follows the expected trend based on the copper valence. Additional useful information related to the mechanism of corrosion is acquired from an examination of the surface microstructure of water-degraded $YBa_2Cu_3O_{7-x}$ samples. Accordingly, inter- and intragrain cracking phenomena occur during water degradation of $YBa_2Cu_3O_{7-x}$ specimens and serve to enhance the rate of decomposition of the high-T_c lattice. Interestingly, the surface microstructure of corroded samples reveals features which appear to be related to the twinning structure of the host lattice.

Introduction

The high-temperature superconductor $YBa_2Cu_3O_{7-x}$ is known to react with water and carbon dioxide leading to the decomposition of the lattice into $BaCO_3$, CuO and Y_2BaCuO_5.[1-10] The especially high reactivity exhibited by the ceramic oxide material has been attributed to the high formal oxidation state of copper (i.e., +2.33) and to the presence of reactive alkaline earth components in the structure.[3,6-9] In addition, lattice defects and surface imperfections are believed to contribute to the high reactivity.[3]

It is now commonly accepted that the oxygen stoichiometry of cuprate superconductors is one of the most crucial parameters controlling conductive and superconductive properties of these compounds. Oxygen content for $YBa_2Cu_3O_{7-x}$ samples normally varies over the range of $0 < x < 1$.[11-13] The more highly oxygenated materials exhibit orthorhombic structures with varying amounts of oxygen vacancies at the O(4) $(0,{}^1/_2,0)$ and O(5) $({}^1/_2,0,0)$ sites. Structures containing 2-, 3-, and 4-fold coordinated Cu(1) sites in ordered oxygen arrays have been identified for $YBa_2Cu_3O_{7-x}$ samples having $6.58 > 7 - x > 6.45$.[13,14] In the tetragonal $YBa_2Cu_3O_6$ phase, oxygen atoms are completely absent at the O(4) and O(5) sites.[11,15,16]

The bond lengths in $YBa_2Cu_3O_{7-x}$ samples deviate from those expected from chemical considerations. Consequently, the Ba–O distance is too large for the Cu–O framework at $x = 0$ and too small for the structure at $x = 1.0$. The structural requirement that the Ba–O and Cu–O layers be commensurate leads to a situation where internal strain exists within the lattice. At $x = 0$, the structure relieves the majority of the strain by transferring charge between the two crystallographically distinct copper sites. For the completely oxygen deficient material, $YBa_2Cu_3O_6$, the mechanism is less effective leaving the lattice with a significant amount of internal strain.[17]

Within the $YBa_2Cu_3O_{7-x}$ system, superconductivity is normally found for orthorhombic materials having $6.35 < 7 - x < 7.00$. Systematic studies of $YBa_2Cu_3O_{7-x}$ samples with different oxygen contents have shown that the superconductive transition temperature (T_c) values tend to cluster around 90 K for $6.84 < 7 - x < 7.0$ and around 60 K for $6.40 < 7 - x < 6.60$. In addition, the lattice parameters have been shown to be directly coupled to the oxygen content. A distinct steplike increase in the c-axis length occurs close to $x = 0.6$, the exact value of which depends on the annealing temperature.[13] The cell volume for the tetragonal materials is ~1.6% larger than that for the analogous orthorhombic phase. Since the $YBa_2Cu_3O_{7-x}$ samples are typically prepared via solid state routes which involve heating metal oxides and carbonate salts to temperatures in excess of 900 °C, structural instabilities are expected to occur when the samples are cooled back

(1) Rosamila, J. M.; Miller, B.; Shneemeyer, L. F.; Waszczak, J. V.; O'Bryan, H. M., Jr. *J. Electrochem. Soc.* **1987**, *134*, 1863.
(2) Magee, V. M.; Rosamila, J. M.; Kometani, T. Y.; Schneemeyer, L. F.; Waszczak, J. V.; Miller, B. *J. Electrochem. soc.* **1988**, *135*, 3026.
(3) Thompson, J. G.; Hyde, B. G.; Withers, R. L.; Anderson, J. S.; Fitzgerald, J. D.; Bitmead, J.; Paterson, M. S.; Stewart, A. M. *Mater. Res. Bull.*, **1987**, *22*, 1715.
(4) McDevitt, J. T.; Longmire, M.; Gollmar, R.; Jernigan, J. C.; Dalton, E. F.; McCarley, R.; Murray, R. W.; Little, W. A.; Yee, G. T.; Holcomb, M. J.; Hutchison, J. E.; Collman, J. P. *J. Electroanal. Chem.* **1988**, *243*, 465.
(5) Riley, D. R.; McDevitt, J. T. *J. Electroanal. Chem.* **1990**, *295*, 373.
(6) Bachtler, H.; Lorenz, W. J.; Schindler, W.; Saemann-Ischenko, G. *J. Electrochem. Soc.* **1990**, *135*, 2284.
(7) Yan, M. F.; Barns, R. L.; O'Bryan, H. M. Jr.; Gallagher, P. K.; Sherwood, R. C.; Jin, S. *Appl. Phys. Lett.* **1987**, *51*, 532.
(8) Bansal N. P.; Sandkuhl, A. L. *Appl. Phys. Lett.* **1987**, *51*, 532.
(9) Gallagher, P. K.; Grader, G. S.; O'Bryan, H. M. Jr. *Mater. Res. Bull.* **1988**, *23*, 1491.
(10) Gao, Y.; Merkel, K. L.; Zhang, C.; Balachandran, U.; Poeppel, R. *J. Mater. Res.* **1990**, *5*, 1363.
(11) Gallagher, P. K. *Adv. Ceram. Mater.* **1987**, *2*, 565.
(12) Nakazawa, Y. and Ishikawa, M. *Phys. C* **1989**, *158*, 381.
(13) Cava, R. J.; Hewat, A. W.; Hewat, E. A.; Batlogg, B.; Marezio, M.; Rabe, K. M.; Krajewski, J. J.; Peck, W. F., Jr.; Rupp, L. W., Jr. *Phys. C* **1990**, *165*, 419.
(14) Beyers, R.; Ahn, B. T.; Gorman, G.; Lee, V. Y.; Parkin, S. S. P.; Ramirez, M. L.; Roche, K. P.; Vazquez, J. E.; Gur, T. M.; Huggins, R. A. *Nature* **1989**, *340*, 619.
(15) Santoro, A.; Miraglia, S.; Beech, F.; Sunshine, S. A.; Murphy, D. W.; Shneemeyer, L. F.; Waszczak, J. V. *Mater. Res. Bull.* **1987**, *22*, 1007.
(16) Izumi, F.; Asano, H.; Ishigaki, T.; Takayama-Muromachi, E.; Uchida, Y.; Watanaba, N.; Nishikawa, T. *Jpn. J. Appl. Phys.* **1987**, *26*, L649.
(17) Brown, I. D. *Solid State Chem.* **1991**, *90*, 155.

0897-4756/93/2805-0361$04.00/0

to room temperature.[12,13] Accordingly, the volume contraction which occurs upon cooling results in transformational stresses in the orthorhombic grains. An elongation of the *b* axis and a contraction of the *a* axis result from this structural change. The resultant strains are thought to be accommodated mainly by twinning shear on {110}-type planes.[18-20] In most cases, twinned microstructures are produced with parallel boundaries. Interestingly, the thickness of each twin boundary layer (parallel to [001]) is comparable to the coherence length (i.e., ~34 Å); the length and width of the twin boundaries depends on the local oxygen content.[21,22]

Although the reaction of $YBa_2Cu_3O_7$ with water has been well characterized to date,[1-10] by comparison, little information is available currently concerning the water degradation characteristics of the oxygen deficient forms of $YBa_2Cu_3O_{7-x}$. Early work with samples of unknown oxygen content completed by Thompson et al.[3] showed that the tetragonal forms of the high-T_c material degrade more rapidly than the more highly oxygenated orthorhombic forms. The higher reactivity of the tetragonal material was attributed to the larger concentration of oxygen vacancies in the compound.

In the present study, we explore the effect that oxygen content has on the rate of the corrosion decomposition of $YBa_2Cu_3O_{7-x}$ system. Three samples of well defined oxygen content, $YBa_2Cu_3O_{7.00}$, $YBa_2Cu_3O_{6.59}$, and $YBa_2Cu_3O_{6.05}$ are analyzed in this regard. In addition, we show that the surface microstructure of the water degraded samples provides useful information related to the twin and defect structures within this superconducting material.

Experimental Procedure

A large batch of the fully oxygenated $YBa_2Cu_3O_{7.00}$ material was prepared via a solid state reaction at 935 °C with several intermediate grindings. Pellets 1 mm thick and 13 mm wide in diameter were formed and sintered at 935 °C. The $YBa_2Cu_3O_{7.00}$ samples were annealed at 430 °C for 48 h in flowing oxygen. Specimens of $YBa_2Cu_3O_{6.05}$ were obtained by heating the fully oxygenated pellets in flowing argon at 850 °C for 4 h and then cooling to room temperature at a rate of 150 °C/h. Samples of $YBa_2Cu_3O_{6.59}$ were prepared in a similar fashion by heating in flowing argon $YBa_2Cu_3O_{7.00}$ at 430 °C for 3.5 h and cooling to room temperature at a rate of 60 °C/h. The densities of all pellet samples were determined to be ≥80%.

For the corrosion measurements, both powders and pellets of the $YBa_2Cu_3O_{7-x}$ samples were examined. Pellets were soaked in deionized water for variable amounts of time. The powder samples were prepared by grinding disks, mixing 150 mg of the resulting powder with a few drops of acetone, and spreading the powder on a 25 mm × 35 mm glass slide. The actual corrosion measurements conducted with the powder samples were performed by placing the material in a closed chamber that was equilibrated with water vapor held at 75 °C. Samples were removed from the chamber to complete the X-ray analysis. Phase contents for corroded $YBa_2Cu_3O_{7-x}$ samples were estimated using X-ray powder diffraction as described previously.[23]

Information related to the corrosion of $YBa_2Cu_3O_{7-x}$ was obtained using X-ray powder diffraction (XRD; Philips Electronic Instruments, Mount Vernon, New York) with Cu Kα radiation, scanning electron microscopy (SEM; JEOL 35CF, JEOL, Ltd., Tokyo) equipped with an energy-dispersive spectrometer (EDS; Model 8000, Kevex Instruments, San Carlos, CA), and transmission electron microscopy (TEM; JEOL JEM-1200FX, JEOL, LTD, Tokyo). Microscopes were operated at accelerating voltages of 25 and 120 kV, respectively. The oxygen contents for the $YBa_2Cu_3O_{7-x}$ pellets were determined using an iodometric titration method[24] with a reproducibility of ±0.02 oxygens per formula unit. Values of T_c were established with magnetization experiments. Using these methods, the $YBa_2Cu_3O_{7.00}$ material was found to possess an average copper valence of +2.33, T_c = 90 K, unit cell dimensions of a = 3.818, b = 3.889, and c = 11.656; for $YBa_2Cu_3O_{6.59}$, Cu^{n+} = +2.06, T_c = 60K, a = 3.826, b = 3.872, and c = 11.717; and for $YBa_2Cu_3O_{6.05}$, Cu^{n+} = +1.70, nonsuperconducting down to 15 K, $a = b$ = 3.866 and c = 11.870.

Table I. Corrosion Product Distribution for $YBa_2Cu_3O_{7-x}$ Pellet Samples Exposed to Water Solution at 25 °C for 4 Days

compound	estimated phase contents (wt %)[a]			
	$YBa_2Cu_3O_{7-x}$	$BaCO_3$	"Y_2BaCuO_5"	CuO
$YBa_2Cu_3O_{7.00}$[b]	22	9	4	3
$YBa_2Cu_3O_{6.59}$[c]	54	4		
$YBa_2Cu_3O_{6.05}$[d]	0	24		7

[a] The following steps were utilized to estimate the phase contents for the corroded high-T_c samples. A series of $YBa_2Cu_3O_{7-x}$, $BaCO_3$, Y_2BaCuO_5, and CuO specimens were synthesized in phase-pure form. Powder patterns for each of the phases were obtained so as to determine the magnitude of the peak intensity for the major diffraction lines. Relative percentages of the products were estimated by taking the ratio of the peak intensities of the corrosion products to that of the phase pure standard compounds. [b] Before corrosion the number of counts for the most intense peak was 4916. [c] Before corrosion the number of counts for the most intense peak was 2774. [d] Before corrosion the number of counts for the most intense peak was 4331.

Results

Decomposition of fully oxygenated $YBa_2Cu_3O_7$ samples has been described[7] according to the following equation:

$$2YBa_2Cu_3O_7 + 3H_2O \rightarrow Y_2BaCuO_5 + 5CuO + 3Ba(OH)_2 + {}^1/_2O_2 \quad (1)$$

In aqueous solution, $Ba(OH)_2$ is found to leach away from the surface of the high-T_c material and upon reaction with atmospheric CO_2, the barium ions precipitate as $BaCO_3$:

$$Ba(OH)_2 + CO_2 \rightarrow BaCO_3 + H_2O \quad (2)$$

Thus, three insoluble, insulating corrosion products (Y_2BaCuO_5, CuO, and $BaCO_3$) form during the decomposition of fully oxygenated $YBa_2Cu_3O_7$.

Details related to the decomposition of $YBa_2Cu_3O_{7-x}$ pellet samples soaked in aerated water solutions at room temperature for four days are listed in Table I. Similar data for powders specimens that were exposed to water vapor equilibrated at 75 °C for various time intervals are listed in Table II. Results are provided for three samples with oxygen contents of 7.00, 6.59, and 6.05, respectively. From these studies, the only crystalline decomposition products identified by XRD were CuO, $BaCO_3$, and Y_2BaCuO_5. The amount of each of these phases was found to be dependent upon oxygen content (x), sample form (powder vs pellet), and reaction conditions (temperature and phase of water). It is interesting to note that a major fraction of the decomposed lattice structure leads to the formation of amorphous phase(s). In fact, the Y_2BaCuO_5-

(18) Hervieu, M.; Domenges, B.; Michel, C.; Herger, G.; Provost, J.; Raveau, B. *Phys. Rev. B* **1987**, *36*, 3920.
(19) Pande, C. S.; Singh, A. K.; Toth, L.; Gubser, D. U.; Wolf, S. *Phys. Rev. B* **1987**, *36*, 5669.
(20) Moodie, A. F. and Whitfield, H. J. *Ultramicroscopy* **1988**, *24*, 329.
(21) Sarikaya, M.; Kikuchi, R.; Aksay, I. A. *Phys. C* **1988**, *152*, 161.
(22) Shi, D.; Boley, M. S.; Chen, J. G.; Tang, M.; Welp, U.; Kwok, W. K. and Malecki, B. *Supercond. Sci. Technol.* **1989**, *2*, 255.
(23) Zhou, J. P.; McDevitt, J. T. *Chem. Mater.* **1992**, *4*, 953.
(24) Manthiram, A.; Swinnea, J. S.; Sui, Z. T.; Steinfink, H.; Goodenough, J. B. *J. Am. Chem. Soc.* **1987**, *109*, 6667.

Table II. Corrosion Product Distribution for Powder $YBa_2Cu_3O_{7-x}$ Samples Exposed to Water Vapor at 75 °C

	estimated phase contents (wt%)[a]				
time (h)	$YBa_2Cu_3O_{7-x}$	$BaCO_3$	"Y_2BaCuO_5"	CuO	amorphous[b]
		$x = 0.00$			
0.00	100[c]				
5.00	69	9			~22
10.00	47	11	4		~38
20.00	18	13	4	5	60
30.00	3	19	5	5	68
		$x = 0.41$			
0.00	100[d]				
10.00	54	7	8		~31
20.00	21	10	9		~60
30.00	15	11	9	3	62
48.00	5	10	12	4	69
		$x = 0.95$			
0.00	100[e]				
0.20	47	6			~47
0.34	23	6	8		~63
0.83	16	5	7		~72
1.34	2	5	9	2	82
15.00		7	11	2	~80
20.00		14	7	2	~77
30.00		26		4	~70

[a] Phase contents were estimated according to the procedure described in the caption of Table I. [b] Amorphous phase(s) contents were calculated by subtracting the sum of the $YBa_2Cu_3O_{7-x}$, $BaCO_3$, "Y_2BaCuO_5", and CuO phase contents from 100%. [c] Before corrosion the number of counts for the most intense peak was 4916. [d] Before corrosion the number of counts for the most intense peak was 2774. [e] Before corrosion the number of counts for the most intense peak was 4331.

like phase identified by XRD does not show all the diffraction peaks that are normally found for authentic Y_2BaCuO_5 samples.[25] Thus, the phase may be better described as an intermediate "Y_2BaCuO_5" phase. The large fraction of amorphous phase(s) and the presence of this distorted "Y_2BaCuO_5" is not surprising given that these corrosion reactions occur at relatively low temperatures where ion mobility is sufficiently low to prevent formation of the more thermodynamically stable crystalline metal oxide and metal carbonate decomposition products.

A major difference between the solution and the vapor method is that the cation ratio is only preserved with the latter method. Thus, analysis of the product distribution can be completed more readily with the vapor-phase technique.[23] From the data provided in Table II and that presented in Figure 1, the relative reactivities of the different $YBa_2Cu_3O_{7-x}$ samples can be assessed. The starting material in the $YBa_2Cu_3O_{7-x}$ series disappears almost completely after ~1.3 h for $YBa_2Cu_3O_{6.05}$, after ~30 h for $YBa_2Cu_3O_{7.00}$, and after ~48 h for $YBa_2Cu_3O_{6.59}$. Moreover, the relative corrosion reactivities trends obtained for powder samples exposed to water vapor are consistent with those acquired for the pellet samples soaked in solution. Thus, from these data it is evident that the relative order of chemical stability in the $YBa_2Cu_3O_{7-x}$ series is $YBa_2Cu_3O_{6.59} > YBa_2Cu_3O_{7.00} \gg YBa_2Cu_3O_{6.05}$.

Examination of the surface microstructure by scanning electron microscopy of $YBa_2Cu_3O_{7-x}$ samples exposed to water solution and vapor yields useful information related to the mechanism of corrosion in these high-T_c materials.

(25) Steinfink, H.; Swinnea, J. S.; Sui, Z. T.; Hsu, H. M.; Goodenough, J. B. *J. Am. Chem. Soc.* **1987**, *109*, 3348.

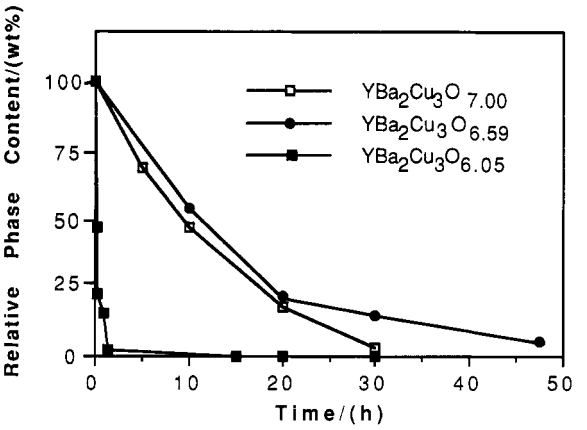

Figure 1. Remaining high-T_c phase content (wt %) for $YBa_2Cu_3O_{7-x}$ powder samples (x = 0.00, 0.41, and 0.95) as a function of exposure time to water vapor equilibrated at 75 °C.

Normally, following water degradation of $YBa_2Cu_3O_{7-x}$, the ceramic samples become coated with fine $BaCO_3$ crystals. However, these crystals can be easily removed by gentle rinsing of the surface of the pellet with acetone to reveal the underlying microstructure. Using such a technique, cracks on the surface of water treated $YBa_2Cu_3O_{7-x}$ were observed by SEM. These cracks form between the grains and their length increases with exposure time to water.

Following longer exposure times, cracking within individual grains is noted. The surface microstructure for a $YBa_2Cu_3O_{6.05}$ sample exposed to water solution for 9 h is shown from top and side perspectives in parts A and B of Figure 2, respectively. The electron micrographs clearly illustrate the preponderance of a large number of thin parallel sheets that coat the surface of the corroded pellet. Parts C and D of Figure 2 show the surface microstructure of $YBa_2Cu_3O_{6.59}$ and $YBa_2Cu_3O_{7.00}$, respectively, following 45-h exposure to water solution. Surface cracking within individual grains is observed for both of these samples. Moreover, thin sheets decorate the surface of each of the corroded ceramic pellets. Interestingly, the two higher oxygen content samples yield sheet facets that intercept at nearly right angles. Moreover, the size of the sheets appears to decrease with increasing oxygen content.

Discussion

Reactivity Trends. The $YBa_2Cu_3O_{7-x}$ compounds are normally synthesized using solid state reaction methods which exploit temperatures above 900 °C. At such high temperatures, the ceramic material initially forms in an oxygen deficient tetragonal crystal habitat with x close to 1.0. If the compound is cooled to room temperature in an oxygen-containing atmosphere, it will take up additional oxygen and will be transformed into an orthorhombic structure which exhibits superconducting properties. Oxygen-deficient samples can be generated easily by two different methods: (1) by synthesizing fully oxygenated $YBa_2Cu_3O_7$ initially and then annealing the material at elevated temperatures in an oxygen deficient environment, or (2) by controlling the oxygen uptake for the freshly synthesized tetragonal material.

The oxygen content varies in the $YBa_2Cu_3O_{7-x}$ series commensurate with a change in the copper formal valence. The compounds examined in this study, $YBa_2Cu_3O_{7.00}$, $YBa_2Cu_3O_{6.59}$, and $YBa_2Cu_3O_{6.05}$ exhibit copper valence

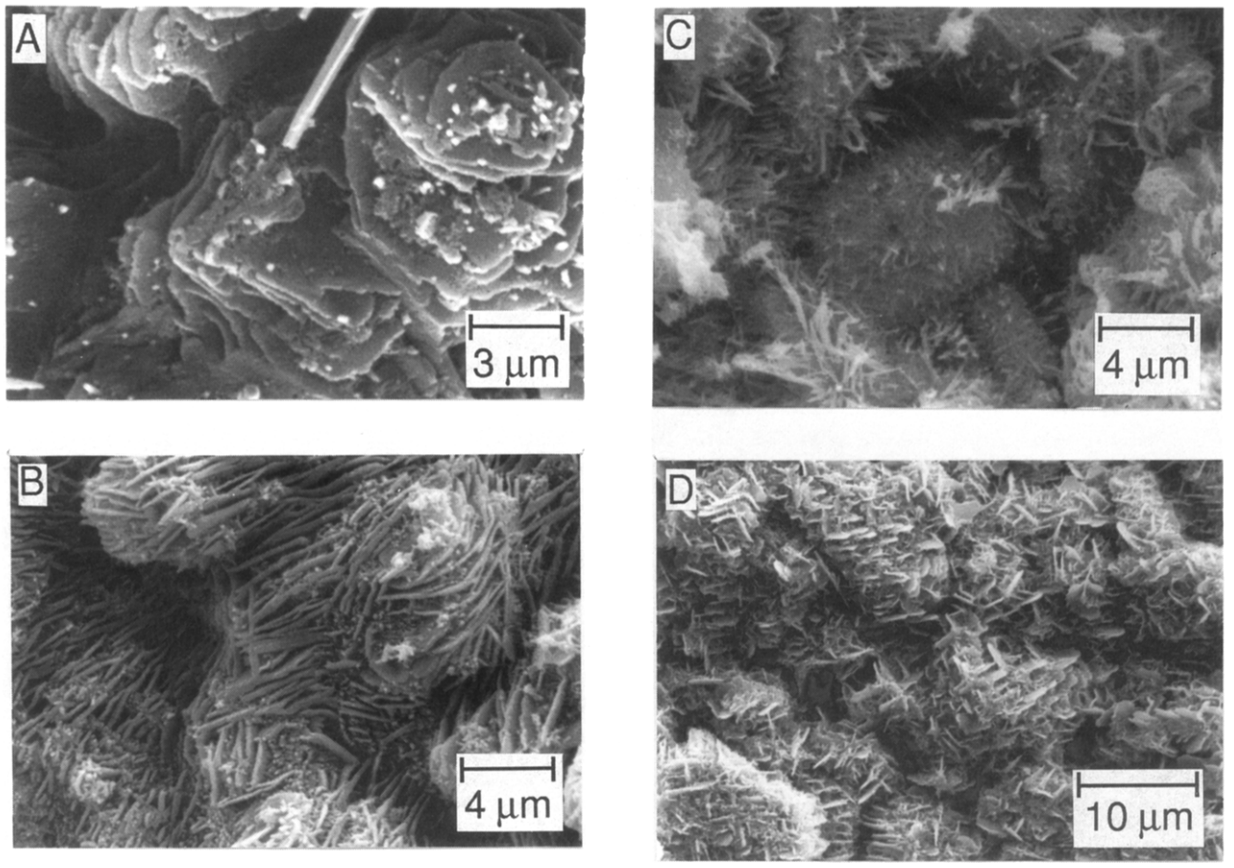

Figure 2. Scanning electron micrographs showing the intra-grain cracking which occurs for $YBa_2Cu_3O_{7-x}$ ceramic pellet samples following their exposure to water solution: (A) top view of $YBa_2Cu_3O_{6.05}$ sample after 9-h exposure, (B) side view of $YBa_2Cu_3O_{6.05}$ sample after 9-h exposure, (C) top view of $YBa_2Cu_3O_{7.00}$ sample after 45-h exposure, and (D) top view of $YBa_2Cu_3O_{6.59}$ sample after 45-h exposure.

values of +2.33, +2.06, and +1.70, respectively. Normal formal valence states for copper are 0, +1, and +2. Thus, those samples which have copper valences ≥2.0 might be expected to behave as strong oxidants and exhibit high chemical reactivity. The fact that evolution of O_2 has been noted previously for $YBa_2Cu_3O_{7.00}$ samples when exposed to water supports this notion.[1,26] Mass spectrometry experiments have confirmed that lattice oxygen rather than water itself is oxidized in the process.[26] For our samples, rapid bubbling of oxygen was observed at the surface of $YBa_2Cu_3O_{7.00}$ when it was soaked in water and slow evolution of gas was noted for the $YBa_2Cu_3O_{6.59}$ sample. Thus, the higher rate of degradation of the fully oxygenated material can be explained in terms of higher percentage of Cu^{3+} sites in the lattice.

The copper valence is not the only important factor responsible for the high reactivity exhibited by these materials. Accordingly, the $YBa_2Cu_3O_{6.05}$ sample which has the lowest copper valence, degrades more rapidly than the two more highly oxidized samples. As mentioned previously in the literature,[3] the higher concentration of oxygen vacancies that are associated with the tetragonal materials may serve to enhance the rate of degradation of the highly oxygen deficient samples. In fact, evidence for the participation of these vacancies in the early stages of corrosion has been identified by proton NMR studies of water degraded $YBa_2Cu_3O_{7-x}$ powders.[27] However, the reactivity trends that we have identified here are not completely consistent with this single explanation. Neither does the copper oxidation state alone satisfactorily explain the unusual reactivity trend.

On the other hand, it can be shown that consideration of internal strain phenomena can account for the observed trend. Estimates[17] of the internal strain that exists in the $YBa_2Cu_3O_{7-x}$ system suggest that minimum strain exists for samples which possess oxygen contents close to 6.6. This result is a direct consequence of the fact that the Ba–O distance is too large for the Cu–O framework for the fully oxygenated compound, $YBa_2Cu_3O_7$, and too small for the fully oxygen depleted material, $YBa_2Cu_3O_6$.

Surface Microstructure. Examination of the surface microstructure of $YBa_2Cu_3O_{7-x}$ samples following their exposure to water reveals important information related to the mechanism of corrosion in this material. The formation of inter- and intragrain cracks is observed for all the $YBa_2Cu_3O_{7-x}$ samples. Such cracks relieve thermal and transformational stresses as the corrosion reactions proceed. Moreover, the cracks serve to enhance the rate of corrosion by providing pathways for water to reach the interior of the sample and by aiding in the diffusion of the corrosion products away from the host material.[28]

The two-dimensional nature of the host lattice strongly influences the degradation properties of $YBa_2Cu_3O_{7-x}$. In fully deoxygenated $YBa_2Cu_3O_{6.00}$ material, the redistribution of charge between the Cu(1) and Cu(2) sites leads

(26) Salvador, P.; Fernandez, E.; Garcia Dominguez, J. A.; Amador, J.; Cascales, C.; Rasines, I. *Solid State Commun.* **1989**, *70*, 71.

(27) Nishihara, H.; Nishida, N.; Takabatake, T.; Kishio, K.; Ohtomo, A.; Hayashi, K.; Ishikawa, M.; Nakazawa, Y.; Koga, K.; Tamegai, T.; Kitazawa, K. *Jpn. J. Appl. Phys.* **1988**, *27*, 1652.

(28) Wang, J.; Stevens, R.; Bultitude, J. *J. Mater. Sci.* **1988**, *23*, 3393.

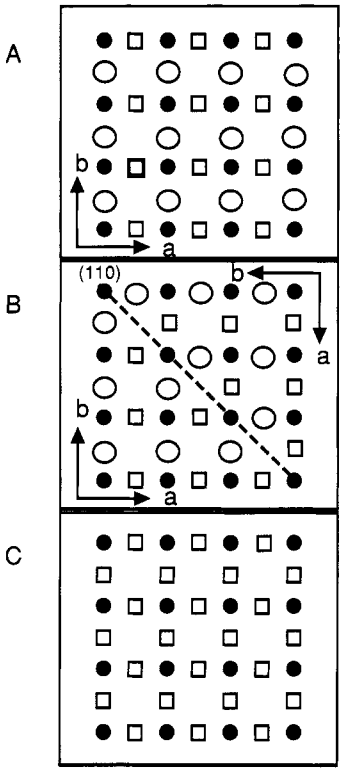

Figure 3. Real-space atomic structure on the (001) plane for various forms of the $YBa_2Cu_3O_{7-x}$ with different oxygen contents. (a) Idealized fully oxygenated orthorhombic $YBa_2Cu_3O_7$ lattice with complete ordering of the oxygen atoms and vacancies in the a–b plane, (b) typical twin structure for orthorhombic $YBa_2Cu_3O_7$ lattice, and (c) diagram for the fully oxygen depleted tetragonal $YBa_2Cu_3O_6$ phase. (●) = copper ions; (○) = oxide ions; (□) = oxygen vacancies.

to changes in the bond lengths. The ratio of the Cu–O distance to the Ba–O distance expected based on chemical considerations (1.368) is incommensurate to the ratio that is dictated by crystal structure (1.414). Thus, the $YBa_2Cu_3O_{6.05}$ structure contains a significant amount of residual strain to accommodate the bond-length mismatch. Consequently, the Ba–O bond must be elongated and the Cu–O bond must be contracted.[17] Similar thermal stress factors are found in the structure along the c axis. Accordingly, microcracks form parallel to the c axis during the corrosion reaction to release these stresses.[28] Moreover, as the lattice decomposes, Ba^{2+} ions are leached away from the structure into the aqueous solution. Electron micrographs of the surface of $YBa_2Cu_3O_{6.05}$ reveal the presence of a series of parallel sheets which suggest that the corrosion occurs most readily along the c axis where the bonding is thought to be the weakest.

The crystal microstructure for the orthorhombic $YBa_2Cu_3O_{7.00}$ and $YBa_2Cu_3O_{6.59}$ materials is more complicated than for the tetragonal $YBa_2Cu_3O_{6.05}$. Associated with the tetragonal to orthorhombic transition are ~1.2–1.8% contractions along the c axis as well as ~1.0–1.2% contractions along the a axis and ~0.2–0.5% expansion along the b axis. The large difference in the thermal expansion characteristics along the a and b axes leads to the formation of internal stresses which are relieved by the formation of twinning structures in the a–b plane. In the absence of such twinning (Figure 3A), a large amount of internal stress would build within the lattice. Microscopic twin boundaries form within individual grains (Figure 3B) separated by [110] planes.[20-22] Thus, each isolated grain in a polycrystalline orthorhombic $YBa_2Cu_3O_{7-x}$ sample is a twinning domain with twin boundaries parallel or perpendicular to each other.[29,30] Splitting of the twin spots along the [110] direction for electron diffraction patterns confirm the presence of the twinning structure for our $YBa_2Cu_3O_{7.00}$ and $YBa_2Cu_3O_{6.59}$ samples. As expected, no twinning structure was observed for the tetragonal $YBa_2Cu_3O_{6.05}$ sample (Figure 3C).

Surface microstructure of corroded $YBa_2Cu_3O_{7.00}$ and $YBa_2Cu_3O_{6.59}$ samples reveal features which are consistent with the presence of twinning microdomains. Most striking is the presence of thin sheets which are connected to each other at nearly right angles. These features likely result from the intersection of two twinning domains along the [110] plane. The fact that larger sheet facets are observed for $YBa_2Cu_3O_{6.59}$ than for $YBa_2Cu_3O_{7.00}$ is consistent with the fact that larger microdomains are generated as oxygen is removed from the orthorhombic lattice [20,21]. Moreover, the intragrain [110] twin boundaries can lead to the formation of subgrain boundaries which serve as defects[29,30] that enhance the rate of corrosion in these materials.[28]

Conclusion

The corrosion behavior in $YBa_2Cu_3O_{7-x}$ compounds has been studied as a function of oxygen content. Within the family of materials, $YBa_2Cu_3O_{6.05}$ is found to degrade most rapidly in the presence of water followed by $YBa_2Cu_3O_{7.00}$ and then by $YBa_2Cu_3O_{6.59}$. Although the copper oxidation state, lattice defects, and concentration of oxygen vacancies are commonly cited as factors which dominate the reactivity of the cuprate compounds, none of these factors alone can explain the unusual reactivity trend. On the other hand, estimates of internal strain phenomena appear, in this case, to explain the observed reactivity trends. Moreover, analysis of the surface microstructure of degraded high-T_c samples has been shown to provide useful information pertaining to twinning structure within the host lattice as well as the lattice decomposition mechanism.

Acknowledgment. This research was supported by the National Science Foundation, Grant No. DMR-8914476, by the National Association of Corrosion Engineers, and by the Welch Foundation. The authors thank Dr. R. Manoharan, Dr. J. Zhou, Dr. M. Schmerling, Dr. J. T. Markert, Dr. H. Steinfink, and Dr. J. S. Swinnea for use of their facilities. R. J. Cava is acknowledged for helpful discussions. We also wish to thank A. Grassini for proofing the manuscript.

(29) Zhou, J. P.; Dou, S. X.; Liu, H. K.; Sorrell, C. C. *J. Mater. Sci. Lett.* **1989**, *8*, 1147.
(30) Zhou, J. P.; Sorrell, C. C.; Dou, S. X.; Bourdillon, A. J. *Aust. J. Phys.* **1989**, *42*, 419.